

Application of MT Forward Modeling Responses for Time-Lapse Monitoring of the Subsurface Electrical Resistivity Changes

Mahallati, A. R.¹ and Montahaei, M.^{2*}

1. M.Sc. Student, Department of Earth Physics, Institute of Geophysics, University of Tehran, Tehran, Iran

2. Assistant Professor, Department of Earth Physics, Institute of Geophysics, University of Tehran, Tehran, Iran

(Received: 16 April 2019, Accepted: 1 Oct 2019)

Abstract

Monitoring fracture developments in the rupture area of an earthquake or unconventional energy reservoirs (ex: enhanced geothermal systems (EGS), coal seam gas (CGS) or shale- gas reservoirs, where massive fluid injection enhances ground permeability) are crucial to determine the stress field direction and optimize well placement and energy production. In addition to microseismic tomography, magnetotelluric (MT) monitoring method provides an independent verification tool to determine more constraints on fluid distribution and migration in target lithologies.

MT phase tensors (PT) and apparent resistivity tensors (RT) are calculated from impedance tensor. Assuming that geological and geo-engineering processes leave an electrically anisotropic volume in their corresponding damage zones, we investigate the time variation of RT and PT residuals for time-lapse MT monitoring purposes. First, we see how the PT and RT are influenced by layered models containing dipping and azimuthal anisotropy and then two synthetic models, representative of real earth situations including general 2D anisotropic features are studied.

The results of our numerical experiments show that despite the phase tensor ellipses, the real part of apparent resistivity tensor could discriminate between isotropic, azimuthally and generally anisotropic half spaces. Furthermore, the PT and RT residuals provide complementary tools for MT monitoring of the variations in the subsurface electrical resistivity structure. Although PT residuals could confine the anomalous region more accurately, the RT residuals determine whether a conductive or resistive variation has been occurred in the anomalous region.

Keywords: Monitoring, Magnetotelluric, Electrical anisotropy, Phase tensor, Apparent resistivity tensor.

1. Introduction

In recent years, there has been increasing applications of electromagnetic (EM) methods for monitoring purposes (Thiel, 2017). The characteristic that motivates such applications of EM methods is their direct sensitivity to the fluids (with much lower electrical resistivity compared to their surrounding host rock). Low-frequency EM fields applied in the MT method make it a favorable tool for monitoring studies where investigation depths are a few hundred meters to several kilometers. This method has been used successfully for monitoring fracks generated during an earthquake (Honkura et al., 2013), volcanic eruption (Aizawa et al., 2011) or during geo-engineering processes employed at the enhanced geothermal system (EGS) and CO₂ geological storage (Peacock et al., 2012, 2013; McFarlane et al., 2014; Ogaya et al., 2016).

Two types of instrument deployments are usually used for MT monitoring purposes:

continuous and time-lapse deployments; while in the first type, MT stations are run continuously before, during and after the experiment, in the second type the same MT survey is repeated multiple times, before and after the experiment (Thiel, 2017; Peacock, et al., 2013).

Aizawa et al. (2011) investigated time variations in impedance data and 2D inversion models obtained from continuous MT measurements at two stations on Sakurajima volcano, Japan. They showed apparent resistivity and phase variations coincident with the summit direction (measured by tiltmeters), implementing horizontal migration of degassed volatiles through a fracture network. Honkura et al. (2013) focused on the time variations of apparent resistivities, phases and 2D inversion models of the initial and co-seismic stages (based on continuously recorded MT data from 10h before till 5h after the 1999M_w 7.6 Izmit earthquake, as well as collocated

*Corresponding author:

mmontaha@ut.ac.ir

stations, run one month after the earthquake). They observed an abrupt decrease in crustal resistivity related to the earthquake and concluded that the pore pressure causes isolated fluids to be changed into the connected network of fluids.

Peacock et al. (2012, 2013) presented results of time-lapse as well as continuous MT monitoring experiments to scan subsurface fracture connectivity and fluid distribution produced by fluid injection at the Paralana Geothermal System (PGS), South Australia. Their analysis approach focused on the phase information inherent in the PT and employed the elliptical nature of the residual PT to identify the direction through which the largest changes occur. They also applied the RT residuals to show the sign and magnitude of change. However, McFarlane et al. (2014) showed that conventional isotropic MT modeling is unable to accommodate for complexities that present within an EGS, and they used an electrically anisotropic approach to better characterize the damaged zone.

In order to examine the potential of the MT method for monitoring purposes of realistic targets, the sensitivity of MT transfer functions is studied in this paper by forward modeling of synthetic geoelectric base models adopted from real EGS systems and fault zones. For time-lapse monitoring purposes, we combined the approaches suggested by McFarlane et al. (2014) and Peacock et al. (2013). Gradually increasing model complexities, we assumed that the damaged zones generated during the geological or geo-engineering processes are electrically anisotropic and investigate monitoring capabilities of different MT transfer functions.

2. The Properties of MT Transfer Functions

MT method is a passive EM exploration technique, utilizing the naturally time-varying EM fields at the earth's surface to calculate transfer (response) functions, which characterize the subsurface geoelectric structures.

This is based on their EM responses to the electrical currents induced in the earth by magnetic field fluctuations (period < 1s produced by remote thunder storms and those

with longer periods are produced by solar wind variations).

It is assumed that MT fields propagate diffusively within the earth and provide estimations of impedance tensor elements (relating linearly horizontal electric and magnetic field components) at penetration depths corresponding to each individual frequency:

$$\underline{\vec{E}}(\omega) = \underline{\underline{Z}}_h \underline{\vec{H}}(\omega) \quad (1)$$

$$\underline{\underline{Z}}_h = \underline{\underline{X}} + i\underline{\underline{Y}} = \begin{bmatrix} Z_{xx} & Z_{xy} \\ Z_{yx} & Z_{yy} \end{bmatrix} \quad (2)$$

The impedance data are commonly represented by the frequency sounding curves of apparent resistivity and impedance phases:

$$\rho_{ij} = \frac{|Z_{ij}|^2}{\mu_0 \omega} \quad \phi_{ij} = \arg(Z_{ij}) = \text{tg}^{-1} \left(\frac{Y_{ij}}{X_{ij}} \right) \quad (3)$$

where, X and Y are the real and imaginary parts of the impedance tensor, respectively. Caldwell et al. (2004) took a different approach and presented the phase information inherent in the impedance data by the phase tensor (PT):

$$\underline{\underline{\Phi}} = \underline{\underline{X}}^{-1} \underline{\underline{Y}} \quad (4)$$

Some major properties of the PT make it a favorable tool for MT data analysis (Booker, 2014):

- i) Local unresolvable structures are not able to distort this kind of transfer function from those of regional structures.
- ii) It determines the dimensionality and directionality of regional structure without any assumptions about the large scale structure.

The definitions presented in Equation (3) are unrelated extensions of apparent resistivity and impedance phase concepts, as first suggested by Cagniard (1953) for 1D interpretation of MT data, to consider more general 2D or 3D subsurface resistivity structures. In an analogy with exploration techniques based on inhomogeneous EM plane waves (like control source time domain and frequency domain techniques), complex

apparent resistivity tensor (RT) was developed and utilized for the MT data interpretation (Weckman et al., 2003; Brown, 2016):

$$\underline{\underline{\rho}}_h = \left(\frac{i\mu}{\omega} \right) \det(\underline{\underline{Z}}_h) \underline{\underline{Z}}_h (\underline{\underline{Z}}_h^{-1})^{tr} \quad (5)$$

The real and imaginary parts of the RT as well as PT may be treated as independent symmetric tensors and graphically presented by ellipses.

3. Numerical Experiments

In order to test, calibrate and validate the Matlab codes developed for calculating and plotting the PT and RT ellipses and to investigate the pros and cons of RT and PT representation of MT impedance data, we first adopt the simple 1D anisotropic geoelectrical models as suggested by Heise et al. (2006). In the next step, two examples of real earth situations are considered.

In the following examples, we employ the results suggested by Wannamaker (2005) and assume that complexities generated by the preferentially aligned fracture networks in the subsurface structure during an earthquake or hydraulic fracturing of a reservoir, are well accommodated by anisotropic electrical resistivity. Their forward responses are calculated by the finite difference algorithm of Pek and Verner (1997). For monitoring purposes and in order to characterize directional changes associated with variations in subsurface resistivity structure, we applied residual tensor, defined as (Booker, 2014):

$$\underline{\underline{\Delta}} = \underline{\underline{I}} - \frac{1}{2} (\underline{\underline{\hat{\Lambda}}}^{-1} \underline{\underline{\Lambda}} + \underline{\underline{\Lambda}} \underline{\underline{\hat{\Lambda}}}^{-1}) \quad \text{where} \\ \underline{\underline{\Lambda}} = \underline{\underline{\Phi}} \quad \text{or} \quad \underline{\underline{\rho}}_h \quad (6)$$

This compares MT responses before ($\underline{\underline{\Lambda}}$) and after ($\underline{\underline{\hat{\Lambda}}}$) occurrence of the event (geological and geo-engineering processes like: earthquake, hydraulic fracturing ...). Resistivity tensor assigned to each anisotropic layer is symmetric and positive definite and could be diagonalized and revealed by three principal resistivities and three successive rotations around z-axis (by anisotropy strike angle, α_s), then around new

x'-axis (by anisotropy deep angle, α_d) and finally around the newest z''-axis (by anisotropy slant angle, α_l) (Pek and Santos, 2002):

$$\underline{\underline{\rho}} = \begin{pmatrix} \rho_{xx} & \rho_{xy} & \rho_{xz} \\ \rho_{yx} & \rho_{yy} & \rho_{yz} \\ \rho_{zx} & \rho_{zy} & \rho_{zz} \end{pmatrix} = \\ \mathbf{R}_z^t(\alpha_s) \mathbf{R}_{x'}^t(\alpha_d) \mathbf{R}_{z''}^t(\alpha_l) \begin{pmatrix} \rho_x & 0 & 0 \\ 0 & \rho_y & 0 \\ 0 & 0 & \rho_z \end{pmatrix} \\ \mathbf{R}_{z''}(\alpha_l) \mathbf{R}_{x'}(\alpha_d) \mathbf{R}_z(\alpha_s) \quad (7)$$

(superscript t denotes transpose of the matrix).

A detailed investigation of the parameter resolvability based on analyzing the structure of conductivity tensor and the differential equations that the EM fields satisfy in a 1D anisotropic earth model, where one of the horizontal principal axes is common between all layers shows that in these special anisotropic cases, EM fields are decoupled in two independent modes. The diagonal elements of the impedance tensor vanish and its off-diagonal elements are defined by the orthogonal EM field components at the earth surface (Yin, 2003).

Where the anisotropic resistivity tensor is obtained by rotating the principal resistivity axes around the x-axis (dipping anisotropic model) Z_{xy} contains the information about the longitudinal resistivities along the stratification (ρ_l).

The Z_{yx} contains the information about the projection of the principal resistivities on to the horizontal plane. They are defined as (Yin, 2003): $(\rho_l \cos^2 \alpha_d + \rho_t \sin^2 \alpha_d)$ (where ρ_l , ρ_t are resistivities along and perpendicular to the stratification). In azimuthal anisotropic earth model with $\rho_x = \rho_z = \rho_l$ and $\rho_y = \rho_t$ information about the ρ_l , ρ_t would be resolved from Z_{xy} , Z_{yx} components, respectively (Yin, 2003).

3-1. Example 1: Simple Layered Models

We start our synthetic studies from layered models suggested by Heise et al. (2006) resulting that MT phase splits are

consequences of spatial conductivity gradients rather than the intrinsic anisotropy of the conductivity tensor. This could not be used as an MT analogue of shear wave splitting to conclude anisotropy in the lower crust and upper mantle. The anisotropic models and their corresponding phase and apparent resistivity tensor ellipses are presented in Figure 1.

In azimuthally anisotropic half space model (Figure 1a (i)) an off-diagonal tensor:

$$\underline{\underline{Z}} = (1-i) \begin{bmatrix} 0 & Z_{xy} \\ Z_{yx} & 0 \end{bmatrix} \quad (8)$$

represents the impedance tensor at all periods (Yin, 2003). Computations based on Equations (4) and (5) show that phase tensors are circles of unit radius at all periods (Figure 1b (i)). Although the imaginary part of the apparent resistivity tensor vanishes, its real part delineates ellipses elongated parallel to the maximum principal resistivity (Figure 1c-d (i)).

In the next anisotropic models, the impedance tensors are in general form (Marti, 2013):

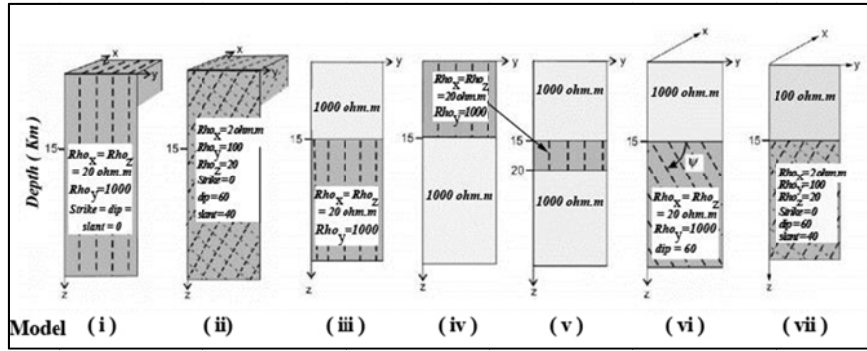
$$\underline{\underline{Z}}_{1D-anis} = \begin{bmatrix} Z_{xx} & Z_{xy} \\ Z_{yx} & -Z_{xx} \end{bmatrix} \quad (9)$$

In generally anisotropic half space (model 1a (ii)) where electrical resistivity is uniform, the phase differences between EM fields are equal in all directions. Also the off diagonal components of the impedance tensor are in phase and the phase tensors are circles of unit radius in all periods (Figure 1b (ii)). However, principal resistivities are not parallel and perpendicular to the surface plane. Accordingly, the ellipses of RT real parts are uniformly deflected with respect to the x, y axes (Figure 1c (ii)), while the ellipses of RT imaginary parts reflect the effect of conductivity heterogeneities on

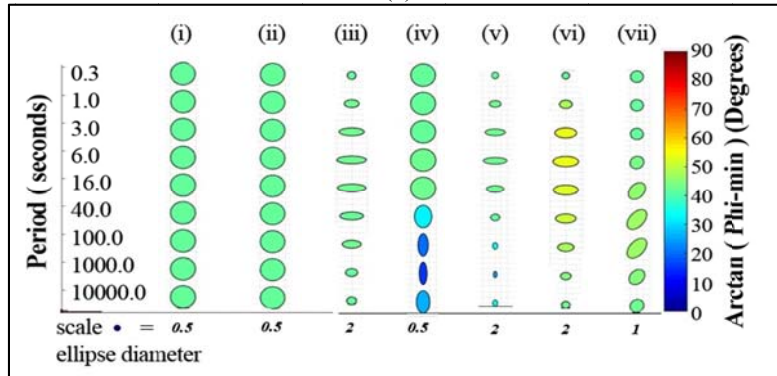
phases (Figure 1d (ii)).

In models (1a (iii-iv)) where MT fields enter the underlying half space from an overburden, phase tensors (Figures 1b (iii-iv)) are representative of uniform upper layers and delineate circles at first and then become ellipses whose major axis are along the direction of decreasing resistivities. In the case of an anisotropic layer in an isotropic background (Figure 1a (v)), phase tensors are sensitive to both the top and bottom of the layer. Their size first increases and then decreases (Figure 1b (v)), according to the resistivity variation along x-direction. In the last two examples where the anisotropy dip angles are non-zero (Figures 1a (vi-vii)), the maximum and minimum horizontal projection of resistivity should be considered. Here, phase tensors are ellipses whose major axis are along the direction of decreasing resistivities (Figures 1b (vi-vii)).

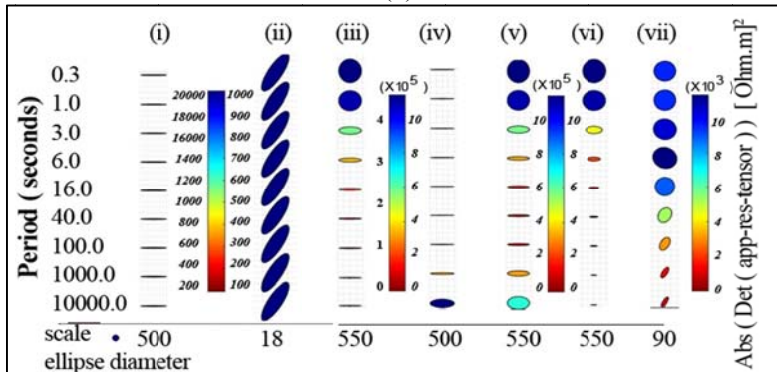
While the imaginary part of the apparent resistivity tensor just reveals the effects of conductivity heterogeneities on the phases. Also its real part represents the overall dissipative behavior of the equivalent model half-space, beneath the observation point and delineates ellipses whose major and minor axis are along the projection of the principal resistivities on to the horizontal plane (Brown, 2016). These are best explained by comparing the behavior of real and imaginary parts of the RT as well as PT ellipses over half spaces, Whereas PT ellipses could not discriminate between isotropic and anisotropic half spaces (Figures 1b (i-ii)) the ellipses of RT real parts show different behavior over isotropic, azimuthally and generally anisotropic half spaces (Figures 1c (i-ii)). In other layered anisotropic models with an isotropic overburden (Figures 1a (iii, V-Vii)) real RTs delineate circles at short periods and at longer periods, they become ellipses oriented along the maximum horizontal resistivities.



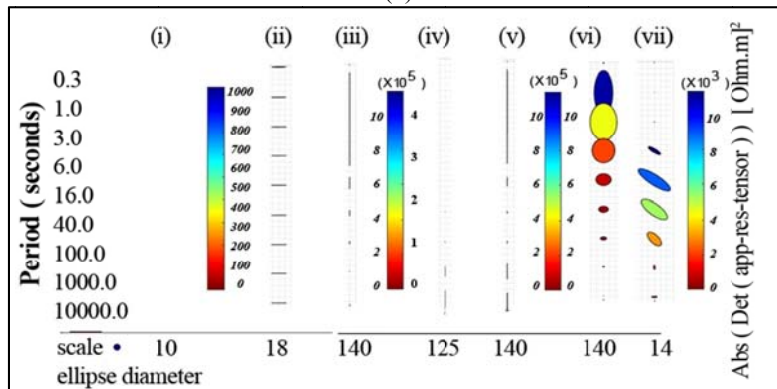
(a)



(b)



(c)



(d)

Figure 1. (a) electrically anisotropic layered models investigated by Heise et al. (2006) and their corresponding phase, real and imaginary apparent resistivity tensors (b, c and d, respectively).

3-2. Example 2

In the next step, we consider an example of enhanced geothermal systems (EGS) from South Australia (Peacock et al., 2013), where

hydraulic fracturing (made by massive fluid injection) stimulates fluid pathways within hot lithologies, that enhances subsurface permeability, maximiz fluid circulation and

results in more efficient energy production. A detailed investigation made by Macfarlane et al. (2014) showed that conventional isotropic MT modeling is unable to simulate geoelectrical structure complexities in an EGS while anisotropic forward modeling could adequately reproduce measured responses. Based on previous geological studies they suggested an initial layered background for the region and assumed that as a consequence of hydraulic fracturing a one-km wide conductive block was developed within the center of the model.

We assumed their proposed layered background for the pre-injection resistivity structure and gradually increase the intricacies of the damaged zone (starting from an isotropic conductive layer evolved to an anisotropic layer and finally into an anisotropic block), updated it to construct post-injection model (Figure 2). This strategy provides us the opportunity to compare the capabilities of different MT transfer functions for monitoring purposes.

Apparent resistivities and impedance phases corresponding to the pre- and post-injection models are presented in Figure 3. While distinct separation between pre and post MT responses are clearly observed for the post-injection models (2A) and (2B), subtle variation in the subsurface electrical resistivity in the model (2C) produces

responses visually indistinguishable from those of pre-injection model. The results also confirm the causality relation between impedance phases and apparent resistivities, indicating that measured changes correspond to the subsurface variation in electrical resistivity.

For comparison purposes, residual apparent resistivity and phase tensor ellipses, calculated between geoelectrical base model and post injection scenarios (Figures 2A, 2B and 2C) are presented in Figures (4-6). The major axis of the residual ellipses coincides with the direction along which greatest change in subsurface electrical resistivity occurs (Heise et al., 2008). Assuming that resistivity changes are isotropic and occur identically in all azimuths (Figure 2A), the residual tensors are presented by circles. In more general cases, where fracture networks generated after fluid injection result in a bulk anisotropic resistivity, the residual tensors are ellipses (Figures 2B and 2C) whose major axis coincides with the direction experiencing greatest change. However, the variations of apparent resistivity and phase transfer functions over an electrical resistivity anomaly contradict each other, where the apparent resistivity is decreased (increased), the phase is increased (decreased), leading to the perpendicular residual apparent resistivity and phase tensor ellipses.

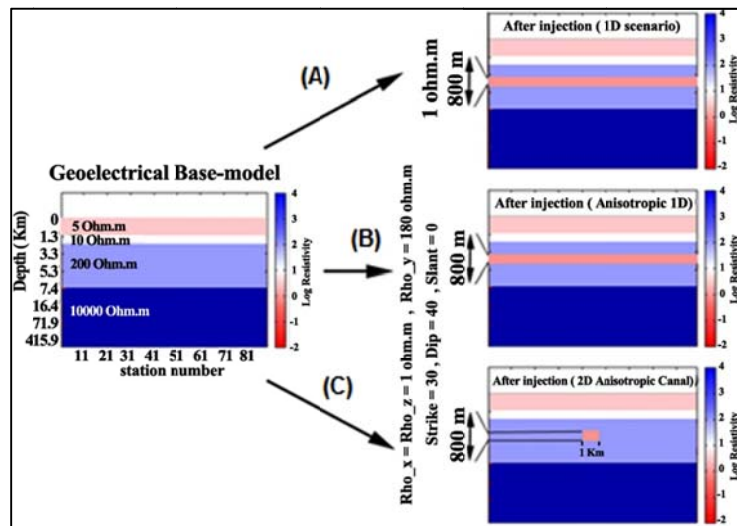


Figure 2. The Geoelectrical base model of Paralana EGS in south Australia suggested by MacFarlane et al. (2014) along with three different post-injection scenarios. Damaged zone generated by hydraulic fracturing is simulated by an isotropic conductive layer in the depth range 3660 m to 4460 m (A) or an anisotropic layer in the same depth range with anisotropy parameters: $\rho_x = \rho_z = 1 \Omega\text{m}$, $\rho_y = 180 \Omega\text{m}$, $\alpha_c = 30^\circ$, $\alpha_D = 40^\circ$, $\alpha_{slant} = 0$ (B) and finally an anisotropic canal of 1 km width (C) developed in the same depth range and with the same anisotropy properties as model (B).

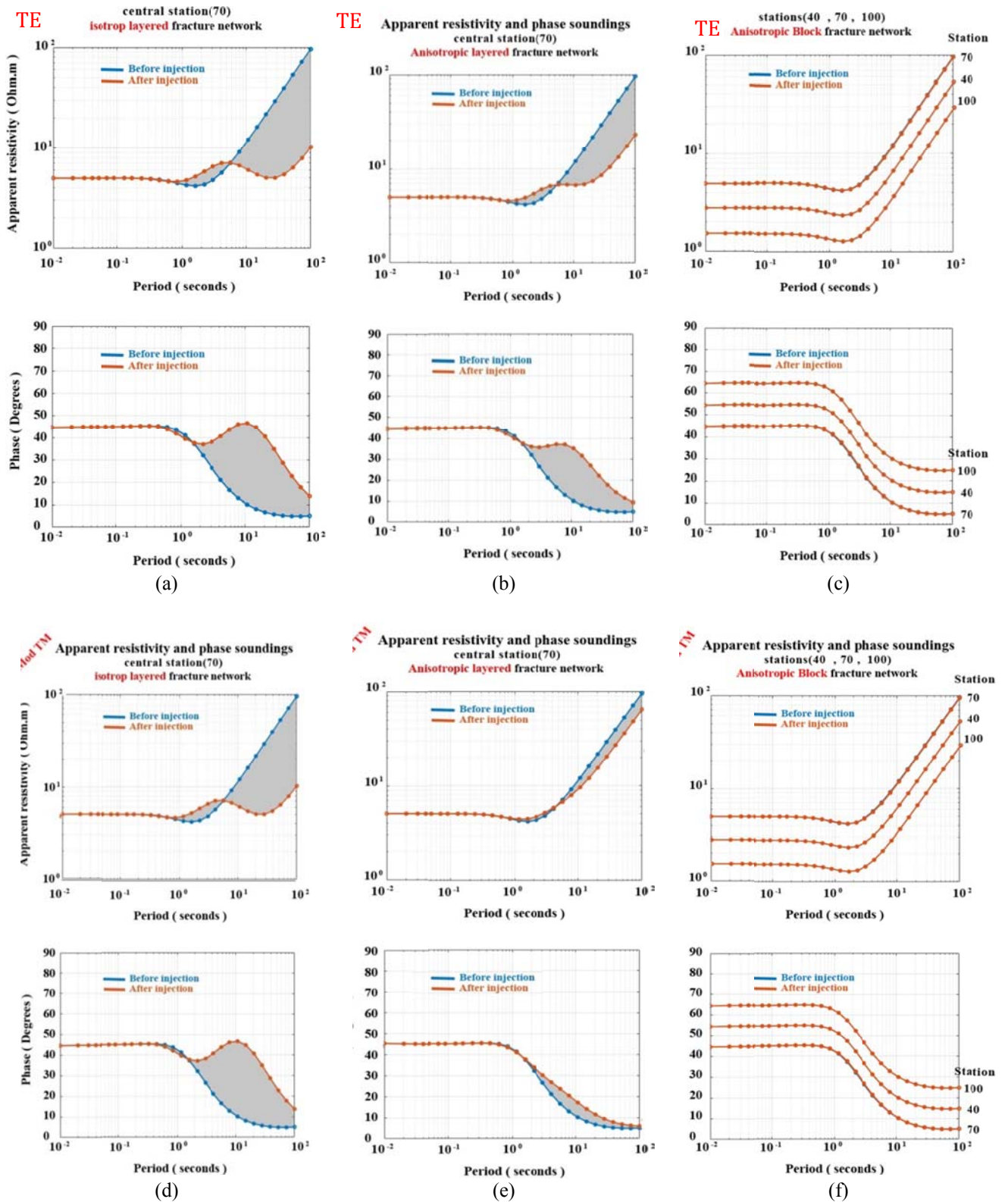


Figure 3. Apparent resistivity and impedance phase pre- and post- injection for the TE and TM modes, corresponding to different scenarios presented in Figure 2. In (c) and (f) the soundings of station 40 and 100 are shifted manually for a better visualization.

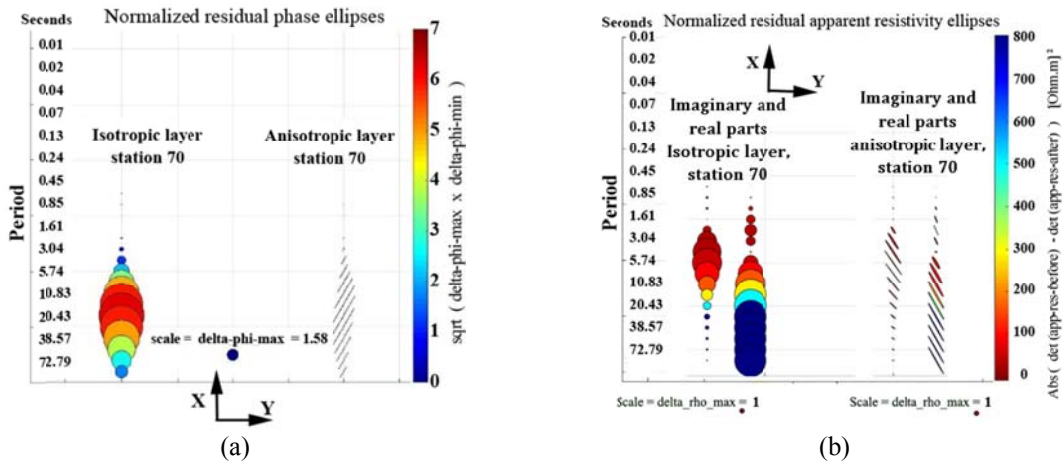


Figure 4. Normalized residual Phase tensor ellipses (a) and normalized residual ellipses of real and imaginary parts of apparent resistivity tensor, (b) calculated over station 70.

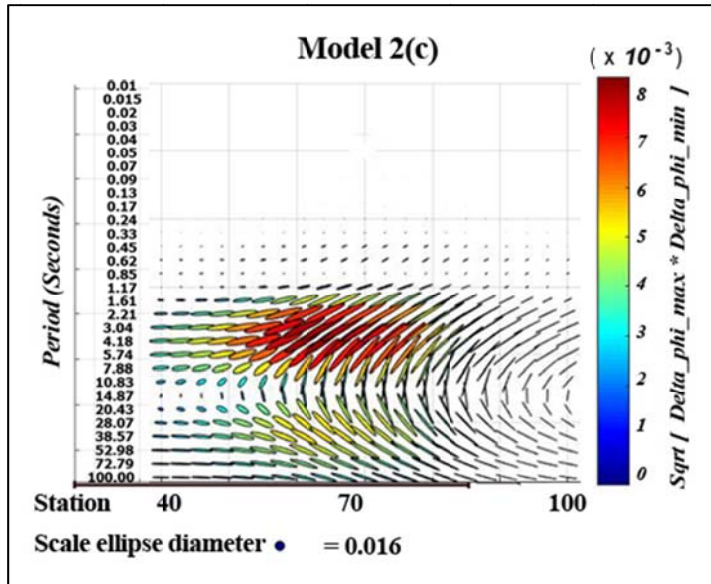


Figure 5. Normalized residual phase tensor ellipses calculated over different stations above the anisotropic canal of Figure 2c.

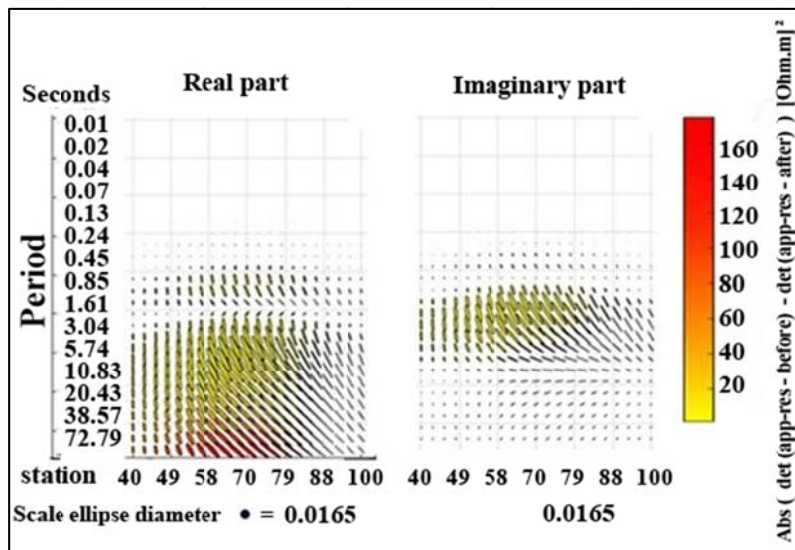


Figure 6. Normalized residual ellipses of real and imaginary part of apparent resistivity tensor calculated over different stations of the geoelectrical model of Figure 2c.

The residual ellipses of PT and imaginary part of the RT respond to both the top and bottom of the anisotropic layer. However, the residual ellipses of the real part RT vary differently. Although with increasing periods, they grow and align along the direction of resistivity change, but at long periods their shape and orientation remain constant and are continuously influenced by the static effects caused by the conductive structure. Thus it is impossible to recognize the underneath structures by this transfer function. Furthermore, the face color of residual PT ellipses indicates the magnitude of resistivity variation but it does not identify whether it has been caused by conductive or resistive structure. Complementary data from the face color of RT tensor ellipses are essential to address this question.

3-3. Example 3: Electrical Resistivity Changes in an Active Fault Zone

Geo-electromagnetic experiments show promising results for monitoring of an active fault zone in terms of imaging variations in subsurface resistivity occurred during an earthquake cycle. Fluid-filled connected networks of fractures developed due to the earthquake rupture in a seismogenic zone produce high electrical resistivity contrasts with their surroundings and made EM methods a typical tool for monitoring electrical resistivity variations in the subsurface. The conductive fractures may be extended to mid-crustal depths beneath major strike-slip faults, necessitating low-frequency EM methods such as MT to monitor resistivity variations in the deep subsurface (Honkura et al., 2013).

We use a synthetic model representative of a fault zone to show how pre- and post-seismic variations in MT responses can be monitored by the residual phase and resistivity tensors. The model consists of a 1 km thick surface layer with 30 Ωm resistivity underlain by a resistive half space of 1000 Ωm . A narrow (0.5 km) very low resistivity (3 Ωm) fault core within a broad (5 km)

conductive (10 Ωm) fault zone are assumed to be located in the centre of the model (Figure 7). The model was first suggested by Eberhardt-Philips et al. (1995) for making inferences about a fault zone based on their seismic tomography and MT responses.

We assumed that a series of micro fractures, preferentially aligned to the north have opened in response to dynamic strains of an earthquake. Following the Wannamaker (2005) the fracture networks within the fault zone are characterized by a 2D anisotropic model with principal resistivities of 10 and 3 Ωm and an anisotropy striking to the 0°.

A comparison of general trend in PT and RT residuals is informative (Figures 8 and 9). Stations above the fault gouge zone observe large changes with PT ellipse orientation pointing perpendicular to the fracture network direction, generated during the earthquake rupture. The size of the PT ellipses increases to a period of ~ 16 s and its face colour becomes redder representing a larger change (~ 30%) then the size decreases and the face colour evolves to blue at later periods, implementing smaller changes. Extending further to the edges of the gouge zone would also result in smaller blue coloured ellipses.

Patterns in calculated RT residual ellipses are well correlated with those of PT. Inside the gouge zone, face colour of the RT residual ellipses shows that the geoelectric variation is conductive along with the rupture direction and farther outside they become redder, representative of larger resistivities.

The ellipses of PT residuals behave more accurately and are sensitive to both the top and bottom of the rupture zone. However, the residuals of the RT real part are persistently influenced up to the largest period of 100 s, resembling the static shift effect produced by the ruptures at long periods. The residuals of the RT imaginary parts also consider the top and bottom of the rupture zone, but their size is much less influenced by the resistivity variations than the PT residuals.

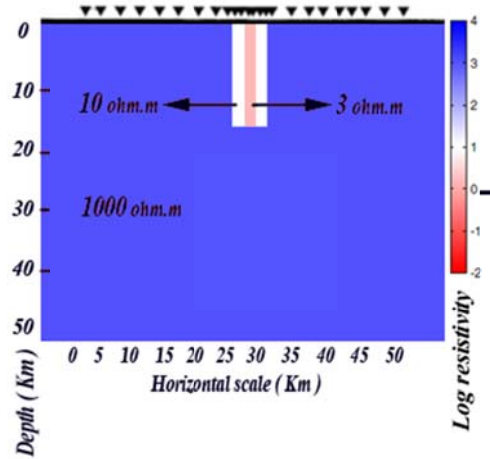


Figure 7. Synthetic fault zone example composed of a uniform resistive (1000 Ωm) upper crust with a 0.5 km wide, 3 Ωm fault core, embedded in a 5 km wide 10 Ωm conductive zone.

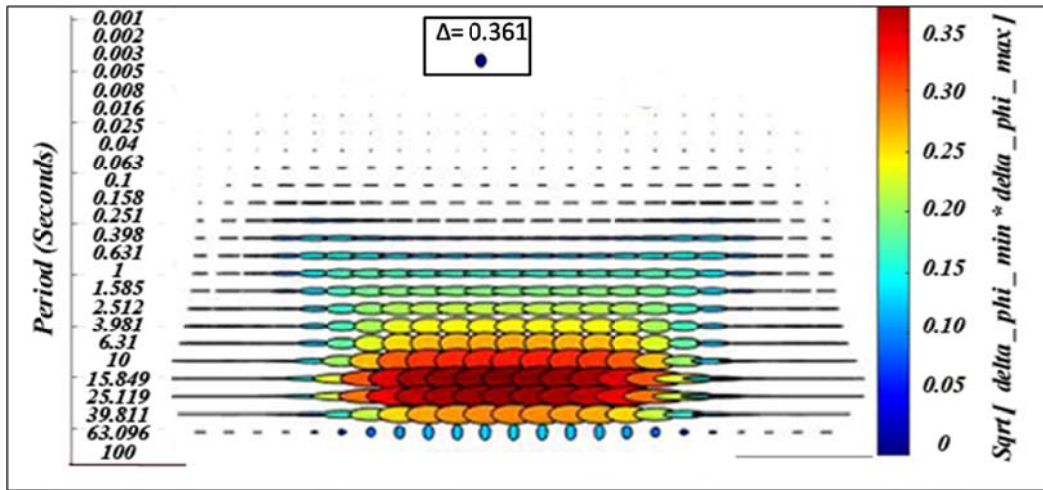


Figure 8. Pseudosections of phase tensor residuals calculated from equation for the fault rupturing scenario presented in Figure 5. The change magnitude calculated as geometric mean of Equation (3) determines the ellipse face colour at each period.

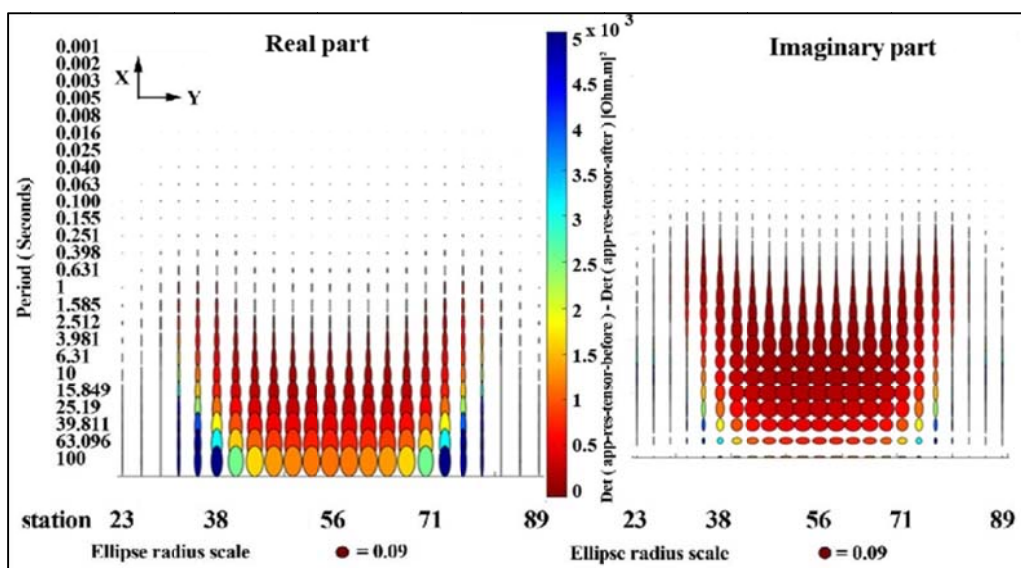


Figure 9. Pseudosections of real and imaginary resistivity tensor residuals calculated from the equation for the fault rupturing scenario presented in Figure 5. The square root of the difference in the RT determinants before and after the earthquake, determines the ellipse facecolor.

4. Conclusion

We assumed that fracture networks opened during an earthquake rupture or massive fluid injections (in unconventional reservoirs like EGS, CSG, ...) are preferentially oriented in a specific direction, enhance the interconnectivity of the fluids and cause the electrical resistivity, primarily controlled by the fluid content, to be anisotropic.

Instead of isotropic modelling, we applied an anisotropic approach to model resistivity variations occurred during a geologic or geo-engineering process. This strategy tries to fully account for the effect of stresses applied by the fluid injection and resembles the real earth situation at the depth of fluid injection or other geo-engineering or geological procedure, more accurately. By gradually increasing the complexities of the damaged zone generated due to the fluid injection (evolved from an isotropic layer to an anisotropic layer and then to a 2D anisotropic block), we examine in more details the monitoring capabilities of different MT transfer functions for subtle and sophisticated resistivity variations occurring in the subsurface.

New findings based on numerical examples investigated in this study with anisotropic forward modelling are as follows:

- Although PT ellipses could not differentiate between isotropic and anisotropic half spaces, but the ellipses of RT real parts are capable to distinguish between isotropic, azimuthally, and generally anisotropic half spaces.

- PT and RT residuals are able to recognize subtle variation in subsurface electrical resistivity that could not affect apparent resistivities and impedance phase soundings.

- 2D anisotropic forward modelling of a synthetic fault zone and an EGS example confirms the previous findings obtained from isotropic forward modelling. Directional dependency of co-seismic changes in crustal resistivity can be successfully imaged by the residual PT and RT ellipses. Although the residuals of imaginary part of the RT and the PT are both sensitive to the top and bottom of the anomalous region, the residuals of the RT real parts are persistently influenced up to the largest period, representing static effect caused by conductive structure. However, their face colour is informative, resembling

whether the geoelectric variation is conductive or resistive.

References

- Aizawa, K., Kanda, W., Ogawa, Y., Iguchi, M., Yokoo, A., Yakiware, H. and Sugano, T., 2011, Temporal changes in electrical resistivity at Sakurajima volcano from continuous magnetotelluric observations. *Journal of volcanology and Geothermal Research*, 199, 165-175.
- Booker, J.R., 2014, The magnetotelluric phase tensor: A critical review. *Surv. Geophys.*, 35, 7–40, doi:10.1007/s10712-013-9234-2.
- Brown, C., 2016, Magnetotelluric tensors, electromagnetic field scattering and distortion in three-dimensional environments. *Journal of Geophysical Research: Solid Earth*, 121(10), 7040-7053.
- Cagniard, L., 1953, Basic theory of the magnetotelluric method of geophysical prospecting. *Geophysics*, 18, 605–645.
- Caldwell, T.G., Bibby, H.M. and Brown, C., 2004, The magnetotelluric phase tensor. *Geophysical Journal International*, 158, 457–469.
- Eberhart-Phillips, D., Stanley, W.D., Rodriguez, B.D. and Lutter, W.J., 1995, Surface seismic and electrical methods to detect fluids related to faulting. *Journal of Geophysical Research: Solid Earth*, 100(B7), 12919-12936.
- Heise, W., Caldwell, T.G., Bibby, H.M. and Brown, C., 2006, Anisotropy and phase splits 625 in magnetotellurics. *Phys. Earth Planet. Inter.*, 158, 107-121.
- Heise, W., Caldwell, T.G., Bibby, H.M. and Bannister, S.C., 2008, Three-dimensional modelling of magnetotelluric data from the Rotokawa geothermal field, Taupo Volcanic Zone, New Zealand. *Geophys J. Int.*, 173, 740–750.
- Honkura, Y., Oshima, N., Matsushima, M., Serif, B., Tuncer, M.K., Tank, S.B., Celic, C. and Ciftci, E. T., 2013, Rapid changes in the electrical state of the 1999 Izmit earthquake rupture zone. *Nat. Commun.*, 4, 2116, doi: 10.1038/ncomms3116.
- Martí, A., 2013, The role of electrical anisotropy in magnetotelluric responses: from modelling and dimensionality analysis to inversion and interpretation.

- Surv. Geophys., 35(1), 179–218.
- McFarlane, J., Thiel, S., Pek, J., Peacock, J. and Heinson, G., 2014, Characterisation of induced fracture networks within an enhanced geothermal system using anisotropic electromagnetic modelling. *J. Volcanol. Geotherm. Res.*, 288, 1–7.
- Ogaya, X., Ledo, J., Queralt, P., Jones, A.G. and Marcuello, A., 2016, A layer stripping approach for monitoring resistivity variations using surface magnetotelluric responses. *J. Appl. Geophys.*, 132, 100–115.
- Pek, J. and Verner, T., 1997, Finite-difference modelling of magnetotelluric fields in two-dimensional anisotropic media. *Geophysical Journal International*, 128, 505–521.
- Pek, J. and Santos, F.A.M., 2002, Magnetotelluric impedances and parametric sensitivities for 1-D anisotropic media. *Comp. Geosci.*, 28, 939–950.
- Peacock, J.R., Thiel, S., Reid, P. and Heinson, G., 2012, Magnetotelluric monitoring of a fluid injection: example from an enhanced geothermal system. *Geophys. Res. Lett.*, 39, L18403, <https://doi.org/10.1029/2012GL053080>.
- Peacock, J.R., Thiel, S., Heinson, G.S. and Reid, P., 2013, Time-lapse magnetotelluric monitoring of an enhanced geothermal system. *Geophysics*, 78, B121–B130.
- Thiel, S., 2017, Electromagnetic monitoring of hydraulic fracturing: relationship to permeability, seismicity and stress. *Surveys in Geophysics*, 38(5), 1133–1169.
- Wannamaker, P., 2005, Anisotropy versus heterogeneity in continental solid Earth electromagnetic studies: fundamental response characteristics and implications for physicochemical state. *Surveys in Geophysics*, 26, 733–765.
- Weckmann, U., Ritter, O. and Haak, V., 2003, Images of the magnetotelluric apparent resistivity tensor. *Geophys. J. Int.*, 155, 456–468.
- Yin, C., 2003, Inherent non-uniqueness in magnetotelluric inversion for 1D anisotropic models. *Geophysics*, 68, 138–146.